Mayer-sampling Monte Carlo calculations of uniquely flexible contributions to virial coefficients

Katherine R. S. Shaul, Andrew J. Schultz, and David A. Kofke[a)]
Department of Chemical and Biological Engineering, University at Buffalo, The State University of New York, Buffalo, New York 14260-4200, USA

(Received 27 June 2011; accepted 19 August 2011; published online 22 September 2011)

We present methods for computing contributions to the virial coefficients uniquely associated with molecular flexibility, and we demonstrate their use with application to the third, fourth, and fifth virial coefficients of united-atom models of linear alkanes and methanol belonging to the suite of transferrable potentials for phase equilibria (TraPPE-UA). We find that these uniquely flexible contributions are more difficult to compute than the remainder of the coefficient, especially for the conditions at which they appear to be most important. The significance of these contributions relative to the full virial coefficient grows with the number of sites (the size of the molecule), the number of molecules, and, to a certain extent, the temperature. The nature of the site-site interactions is of great importance: the significance of the uniquely flexible contribution at third and fourth order is orders of magnitude larger for TraPPE-UA methanol, which has Coulombic interactions, than for TraPPE-UA propane, which does not, even though both models have three sites per molecule and comparable bending potentials. While the uniquely flexible contribution of TraPPE-UA propane has a negligible impact on its third-order virial-equation-of-state estimate of the critical point, the uniquely flexible contribution of TraPPE-UA methanol increases this estimate of its critical pressure by about 5%.
 [doi:10.1063/1.3635773]

I. INTRODUCTION

The virial equation of state (VEOS) is a powerful tool for examination of molecular models. As presented in Eq. (1), P is the pressure, ρ is the density, T is the temperature, and k is Boltzmann's constant. The virial coefficients B_n can be formally defined in terms of molecular interaction energies via the grand-canonical ensemble.[1]

$$\frac{P}{\rho kT} = 1 + \sum_{n=2} B_n \rho^{n-1} \tag{1}$$

Caracciolo *et al*. showed that these definitions are different for rigid and flexible molecular models, and they have derived the uniquely flexible contributions to B_3 and B_4.[2,3] They applied the expressions within the context of a polymer solution, modeled as a lattice for computational convenience. Here, we present and examine uniquely flexible contributions for off-lattice molecular models within the context of low-density vapors, computed via the Mayer-sampling Monte Carlo (MSMC) method.[4,5] We further extend the development to include B_5.

For pairwise-additive models, the virial coefficients B_n are defined in terms of integrals involving the Mayer function, $f_{ij} = \exp(-\beta u_{ij}) - 1$. Within the context of the virial equation of state for dilute gases, u_{ij} is the interaction energy between molecules i and j. For osmotic virial coefficients, the context considered by Caracciolo *et al*.,[2,3] u_{ij} is the potential of mean force between particles i and j within a solvent. Aside from this difference in u_{ij}, expressions for virial coefficients and osmotic virial coefficients are equivalent. The integrals that give B_n from the molecular model are often depicted with a diagram notation in which f_{ij} is drawn as a line between molecules i and j, represented as points. For homogeneous systems such as a bulk fluid, it is acceptable to consider molecule 1 fixed at the origin. Molecule 1 is represented with a white circle, as can be seen in Eq. (2) for B_2, and is referred to as a root molecule. The positions of other molecules $\mathbf{r}_j$ are integration variables, and these molecules are represented with black circles.

$$B_2 = -\frac{1}{2} I_2 = -\frac{1}{2}\int \langle f_{12}\rangle d\mathbf{r}_2 = -\frac{1}{2}$$ (2)

The angled brackets in Eq. (2) denote an ensemble average over the coordinates defining orientation $\boldsymbol{\omega}_j$ and intramolecular degrees of freedom $\boldsymbol{c}_j$, as shown in Eq. (3). If the molecular model is anisotropic, one must average over $\boldsymbol{\omega}_j$ in addition to integrating over $\mathbf{r}_j$, which we define using the molecules' geometric centers. If the molecules have intramolecular degrees of freedom $\boldsymbol{c}_j$, one must also average over these in proportion to the Boltzmann factors associated with their intramolecular energies u_j:

$$\langle f_{12}\rangle = \frac{\int f_{12} e^{-\beta u_1} e^{-\beta u_2} d\boldsymbol{c}_1 d\boldsymbol{c}_2 d\boldsymbol{\omega}_1 d\boldsymbol{\omega}_2}{(\int e^{-\beta u_1} d\boldsymbol{c}_1)(\int d\boldsymbol{\omega}_1)(\int e^{-\beta u_2} d\boldsymbol{c}_2)(\int d\boldsymbol{\omega}_2)}. \tag{3}$$

The Caracciolo *et al*. formulation of B_3 is shown in Eq. (4). We continue their use of I_n to refer to the biconnected diagrams of B_n: the diagrams in which at least two independent paths may be drawn connecting any two molecules in

[a)]Author to whom correspondence should be addressed. Electronic mail: kofke@buffalo.edu.

the diagram. The non-biconnected diagrams of B_n are either singly connected or disconnected. As described in Sec. II, it is advantageous to compute sums of singly connected and disconnected diagrams from a common set of configurations, importance sampled on the sum. To combine the singly connected three-molecule chain and disconnected $-I_2^2$ into one integral T_1 (Eq. (4b)), one must consider a fourth molecule, which we refer to as molecule $1'$. The geometric center of molecule $1'$ may be fixed at the origin like molecule 1, but its intramolecular degrees of freedom are independent from those of molecule 1, as can be seen in Eq. (5). We refer to molecule $1'$ as an *alternate* of molecule 1 and represent it with a gray circle. For rigid molecules, u_i is zero, such that the non-biconnected contribution B_n^{NBC} is zero. Thus, we refer to B_n^{NBC} as the uniquely flexible contribution to B_n. As presented in Eq. (4b), $B_3^{NBC} = -T_1$ measures the sensitivity of the interaction between molecule 1 and molecule 3 to the intramolecular conformation of molecule 1. Note that the conformations sampled by molecule 1 will differ from those sampled by molecule $1'$ because the former interacts with molecule 2, while the latter does not. To the extent that this difference affects interactions with molecule 3, T_1 will be nonzero.

$$B_3 = -\frac{1}{3}I_3 - T_1 \tag{4}$$

$$I_3 = \int \langle f_{12} f_{13} f_{23} \rangle d\mathbf{r}_2 d\mathbf{r}_3 = \tag{4a}$$

$$T_1 = \int \langle f_{12}(f_{13} - f_{1'3}) \rangle d\mathbf{r}_2 d\mathbf{r}_3 = \tag{4b}$$

$$\langle f_{12}(f_{13} - f_{1'3}) \rangle = \frac{\int f_{12}(f_{13} - f_{1'3}) e^{-\beta u_{1'}} e^{-\beta u_1} e^{-\beta u_2} e^{-\beta u_3} d\boldsymbol{c}_{1'} d\boldsymbol{c}_1 d\boldsymbol{c}_2 d\boldsymbol{c}_3 d\boldsymbol{\omega}_1 d\boldsymbol{\omega}_2 d\boldsymbol{\omega}_3}{(\int e^{-\beta u_{1'}} d\boldsymbol{c}_{1'})(\int d\boldsymbol{\omega}_{1'})(\int e^{-\beta u_1} d\boldsymbol{c}_1)(\int d\boldsymbol{\omega}_1)(\int e^{-\beta u_2} d\boldsymbol{c}_2)(\int d\boldsymbol{\omega}_2)(\int e^{-\beta u_3} d\boldsymbol{c}_3)(\int d\boldsymbol{\omega}_3)}. \tag{5}$$

In B_4, there are three singly connected diagrams consisting of all four molecules, which lead to three terms analogous to T_1. The Caracciolo *et al*. formulations of B_4 and its T_i terms are shown below in Eq. (6), where we have rewritten T_i to indicate two alternates of molecule 1: $1'$ and $1''$. Molecule $1''$ is represented with a hatched circle.

$$B_4 = -\frac{1}{8}I_4 - \frac{1}{2}T_2 - \frac{3}{2}T_3 - \frac{3}{2}T_4 + \frac{9}{2}I_2 T_1 \tag{6}$$

$$I_4 = \int \langle f_{12} f_{23} f_{34} f_{14} (3 + 6 f_{13} + f_{13} f_{24}) \rangle d\mathbf{r}_2 d\mathbf{r}_3 d\mathbf{r}_4 \tag{6a}$$

$$T_2 = \int \langle f_{12}(f_{13} f_{14} - f_{1'3} f_{1''4}) \rangle d\mathbf{r}_2 d\mathbf{r}_3 d\mathbf{r}_4 \tag{6b}$$

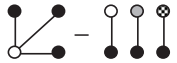

$$T_3 = \int \langle f_{12}(f_{23} f_{34} - f_{1'3} f_{1''4}) \rangle d\mathbf{r}_2 d\mathbf{r}_3 d\mathbf{r}_4 \tag{6c}$$

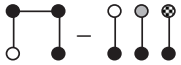

$$T_4 = \int \langle f_{12} f_{23} f_{13} (f_{14} - f_{1'4}) \rangle d\mathbf{r}_2 d\mathbf{r}_3 d\mathbf{r}_4 \tag{6d}$$

In this work, we apply these expressions to off-lattice molecular models. Specifically, we consider the united-atom, transferrable potentials for phase equilibria (TraPPE-UA) for linear alkanes and methanol.[6,7] TraPPE-UA propane and methanol are three-site models that include a bending potential, which imposes an energy penalty when the angle deviates from its equilibrium value. Higher-order TraPPE-UA alkanes include dihedral bending potentials as well. The uniquely flexible contributions for TraPPE-UA alkanes from propane to icosane were presented in the supplementary material of Schultz and Kofke,[8] but the results and computational approach were not discussed in detail. Previously, Shaul *et al*. reported B_2, B_3, and B_4 for TraPPE-UA methanol omitting the uniquely flexible contributions.[9] Additionally, in that work, a rounded value of the oxygen–hydrogen bond length was employed: 0.95 Å instead of 0.945 Å, which is recommended for the model.

This work proceeds as follows. In Sec. II, we detail the Mayer-sampling Monte Carlo method used to compute the uniquely flexible contributions for TraPPE-UA alkanes, as well as the modifications to the approach required for TraPPE-UA methanol because of its Coulombic interactions. We present our results in Sec. III, where we analyze the significance of the uniquely flexible contribution to the virial coefficients and VEOS estimates of the critical point. For TraPPE-UA methanol, we also examine the impact of the

extension of the oxygen–hydrogen bond that resulted from rounding the bond length. We conclude in Sec. IV.

II. METHODS

We employ the overlap-sampling formulation of Mayer-sampling Monte Carlo, described in detail in Ref. 5, to compute B_n and portions thereof. The method employs a hypothetical overlap system having integrands intermediate between that of the target integral, evaluated with a TraPPE-UA potential, and that of the reference integral, evaluated with a hard-sphere potential. Each molecule in the reference is a single hard sphere, regardless of the number of atoms in the target potential. To compute the biconnected contributions B_n^{BC}, we employ the corresponding hard-sphere virial coefficient as the reference integral. To compute the non-biconnected contributions B_n^{NBC}, we employ the singly connected diagrams evaluated for hard spheres as the reference integral for up to fifth order, and, at fifth order, we employ B_5 for hard spheres as the reference integral. The calculation is not particularly sensitive to the choice of the hard-sphere diameter, and we employ the same hard-sphere diameters used previously for the biconnected contributions: 5 Å for TraPPE-UA methanol, 5.25 Å for TraPPE-UA propane, 5.75 Å for TraPPE-UA *n*-butane, and 9.75 Å for TraPPE-UA *n*-dodecane.

Caracciolo *et al*. observed that the components of the uniquely flexible contribution largely cancel one another. In Monte Carlo calculations, small magnitudes often translate to small standard errors, and we have observed that direct computation of T_1, for example, is more efficient with regard to minimizing statistical uncertainty than independent computation of the three-molecule chain and I_2. However, computing T_1 with one MSMC calculation is slightly more complicated because of the presence of molecule 1′. For the three-site TraPPE-UA models of propane and methanol, it is relatively simple to pair the orientations of molecules 1 and 1′ by restricting the molecules to the same plane and the bisector of their angles to the same vector, as shown in Fig. 1. This roughly minimizes the integrand of T_1 at each step, and permits the calculation to focus appropriately on the difference of the intramolecular conformations of 1 and 1′. The improvement in sampling efficiency is considerable, and we apply this restriction at all orders considered. One may similarly attempt to pair the orientations of 1 and 1′ for TraPPE-UA *n*-butane and larger alkanes, but we have not done so in this work. Additionally, for all of the models considered here, we permute the two root molecules and compute the value of T_1 via the average shown in Eq. (7). We denote this formulation as F_3, but it has the same value as T_1. From this formulation, one can see that the uniquely flexible contribution arises from the correlation of differences in the interactions due to different conformations of molecule 1 (i.e., 1 and 1′):

$$F_3 = \frac{1}{2}\int\langle(f_{12}-f_{1'2})(f_{13}-f_{1'3})\rangle d\mathbf{r}_2 d\mathbf{r}_3 = \frac{1}{2}\left(\quad - \quad + \quad - \quad\right) \tag{7}$$

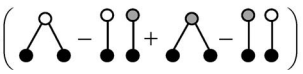

Any of the molecules represented in the diagrams may be the root molecule or its alternate because the system is homogeneous. Consequently, we may make our selection in order to maximize the similarity of the integrands of the singly connected and disconnected diagrams, and thus maximize the computational efficiency. To avoid the need for a second alternate of molecule 1 in B_4, molecule 1″, we employ the expression for B_4 shown in Eq. (8). F_4^C has the same value as T_4, but F_4^A and F_4^B differ quantitatively from T_2 and T_3, respectively, despite containing the same singly connected diagrams. We compute B_4^{NBC} using independent MSMC calculations for I_2, F_3, and $-1/2F_4^A - 3/2F_4^B - 3/2F_4^C$:

$$B_4 = -\frac{1}{8}I_4 + \left(-\frac{1}{2}F_4^A - \frac{3}{2}F_4^B - \frac{3}{2}F_4^C\right) + \frac{5}{2}I_2F_3 \tag{8}$$

$$F_4^A = \frac{1}{2}\int\langle(f_{12}f_{13}-f_{1'2}f_{1'3})(f_{14}-f_{1'4})\rangle d\mathbf{r}_2 d\mathbf{r}_3 d\mathbf{r}_4 = \frac{1}{2}\left(\quad - \quad + \quad - \quad\right) \tag{8a}$$

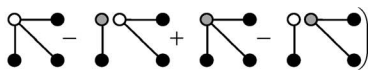

$$F_4^B = \frac{1}{2}\int\langle(f_{12}-f_{1'2})f_{23}(f_{14}-f_{1'4})\rangle d\mathbf{r}_2 d\mathbf{r}_3 d\mathbf{r}_4 = \frac{1}{2}\left(\quad - \quad + \quad - \quad\right) \tag{8b}$$

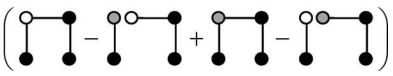

$$F_4^C = \frac{1}{2}\int\langle(f_{12}f_{13}-f_{1'2}f_{1'3})f_{23}(f_{14}-f_{1'4})\rangle d\mathbf{r}_2 d\mathbf{r}_3 d\mathbf{r}_4 = \frac{1}{2}\left(\quad - \quad + \quad - \quad\right) \tag{8c}$$

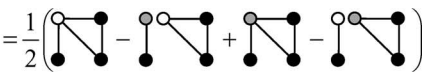

In B_5, there are 11 singly connected diagrams consisting of all five molecules, which lead to 11 terms F_5^i analogous to F_5. We have selected the root molecules as indicated in Eq. (9). We do not show the permutations of molecules 1 and

$1'$ in Eq. (9), but these are included within our calculations. We compute B_5^{NBC} using independent MSMC calculations for I_2, I_3, F_3, $1/2F_4^A + 6F_4^B + 3F_4^C$, and the sum of the F_5^i terms F_5, presented in Eq. (9b).

$$B_5 = -\frac{1}{30}I_5 - F_5 + I_2\left(\frac{1}{2}F_4^A + 6F_4^B + 3F_4^C\right) + F_3\left(3I_3 + \frac{9}{2}F_3 - \frac{5}{2}I_2^2\right) \tag{9}$$

$I_5 =$ 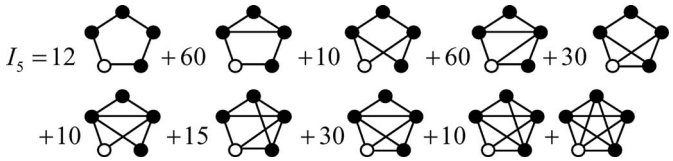 (9a)

$$F_5 = \frac{2}{3}F_5^A + 2F_5^B + 2F_5^C + \frac{1}{2}F_5^D + 2F_5^E + 2F_5^F + 2F_5^G + F_5^H + 2F_5^I + 2F_5^J + \frac{1}{6}F_5^K \tag{9b}$$

$F_5^A =$ 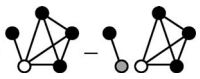 (9ba)

$F_5^B =$ 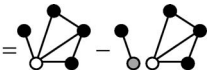 (9bb)

$F_5^C =$ 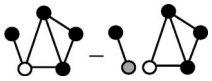 (9bc)

$F_5^D =$ 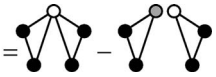 (9bd)

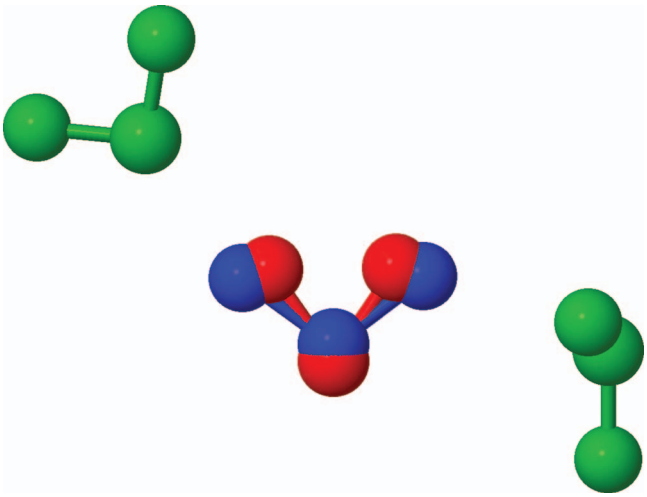

FIG. 1. Snapshot of B_3 calculation (reference-system Markov chain) for TraPPE-UA propane at 1500 K. Molecule 1 is blue and molecule $1'$ (alternate root with same geometric center and paired orientation) is red. Molecules 2 and 3 to left and right are green.

$F_5^E =$ 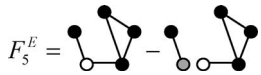 (9be)

$F_5^F =$ 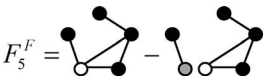 (9bf)

$F_5^G =$ 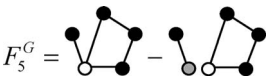 (9bg)

$F_5^H =$ 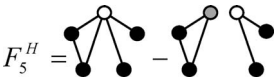 (9bh)

$F_5^I =$ 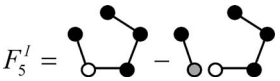 (9bi)

$F_5^J =$ 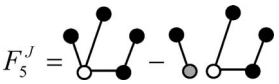 (9bj)

$F_5^K =$ 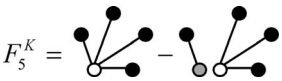 (9bk)

For computations of portions of B_n for TraPPE-UA alkanes, the total number of sampled configurations varied considerably with the size of the molecule and the order n.[8] At least five independent calculations were performed for each case, and each independent calculation sampled at least 10^8 configurations. For computations of B_n^{NBC} for TraPPE-UA methanol, 100 independent calculations of 10^8 steps were performed for each pairing of temperature and order. For all models considered, an additional 7.5% of the number of samples was devoted to the equilibration period for each independent calculation, and the quoted confidence limits are based on the standard error of the mean of the independent calculations.

The point charges of TraPPE-UA methanol introduce complications, which we treat as in previous work for

TraPPE-UA methanol B_2 and higher-order coefficients of the Gaussian charge polarizable model of water.[5,9] At separation distances r where the pair interaction is dominated by the dipole-dipole contribution, the sampling weight of B_2 (the absolute value of the integrand prior to taking the orientational average) diminishes with r^{-3}, a much slower rate of decay than that of the orientationally averaged dipole-dipole interaction, which decays with r^{-6}. Applying a coarse orientational average at each step permits us to achieve this appropriately faster rate of decay. For B_2, this coarse orientational average is the average of four configurations: the nominal (proposed) configuration, the two configurations where only one of the molecules is "flipped" about its geometric center, and the configuration where both are flipped.

The biconnected parts of higher-order B_n would not benefit from this coarse orientational average because the connectivity sufficiently restricts the separation distances considered. The non-biconnected contributions B_n^{NBC}, however, have an even greater need for this procedure than B_2. For B_3^{NBC} and B_4^{NBC}, we average over 2^3 and 2^4 configurations, respectively, where molecule $1'$ is always flipped with molecule 1 to keep their orientations paired. The coarse orientational average proves insufficient for the linear chain of four molecules belonging to F_4^B: molecule 2, bonded to the root, and molecule 3, bonded only to molecule 2, are able to migrate together far from the origin and remain far for many consecutive steps. To avoid this sampling inefficiency, we compute F_4^B with a slightly different approach, in which molecule 3 is moved to preserve its orientation and position relative to molecule 2, and thus the value of f_{23}, whenever molecule 2 is flipped. The presence of f_{13} in F_4^C prevents the need for this procedure by anchoring molecule 3 to the origin, but it also precludes its use, because, if the position of 3 were moved with 2, f_{13} could change substantially and prevent cancellation. Additionally, we do not flip the root molecules when computing F_4^B as it does not provide any advantage with regard to achieving cancellation, despite providing a less coarse orientational average.

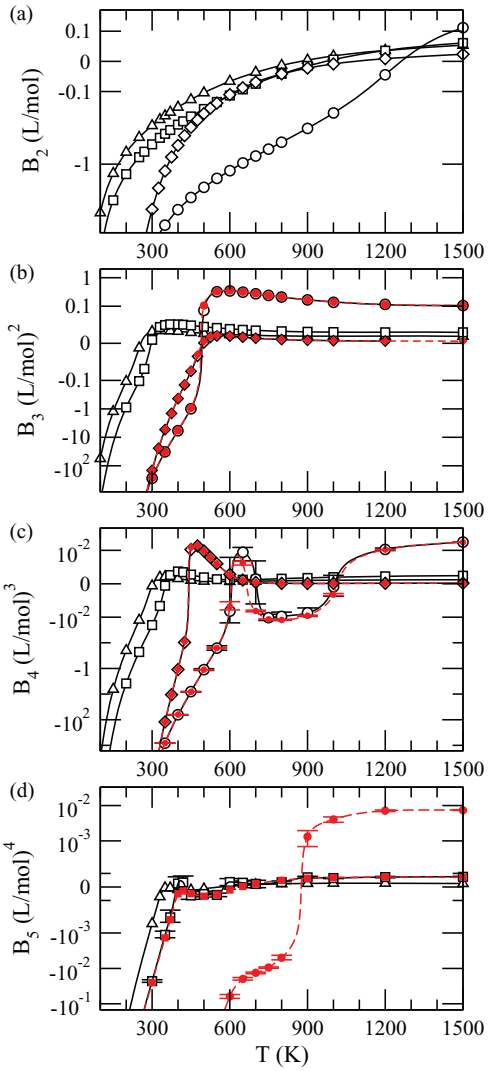

FIG. 2. Virial coefficients for TraPPE-UA propane (triangles), *n*-butane (squares), *n*-dodecane (circles), and methanol (diamonds) at (a) second order, (b) third order, (c) fourth order, and (d) fifth order. Symbols are values computed by MSMC and lines are interpolated using the method of Schultz and Kofke (see Ref. 13). White symbols represent total values, while red symbols represent biconnected contributions. Error bars denote 68% confidence limits where they are not smaller than the symbols.

III. RESULTS AND DISCUSSION

A. Virial coefficients

We present virial coefficients B_n and components thereof for the TraPPE-UA models of propane, *n*-butane, *n*-dodecane, and methanol at third through fifth order. Tabulated values are provided in the supplementary material.[10] TraPPE-UA methanol was not considered at fifth order, and the non-biconnected contribution at fifth order B_5^{NBC} was neglected for alkanes with more than five carbons. In Fig. 2, we plot B_n in black, using an asinh scale that facilitates examination of the temperature dependence across the considered temperature range.

We include B_2 in Fig. 2(a) as a point of reference, even though it has no uniquely flexible contributions. As the TraPPE-UA alkane chain length increases, and the number of site-site interactions between the two molecules increases, the magnitude of B_2 increases. Though TraPPE-UA methanol has three sites, like TraPPE-UA propane, its B_2 values are significantly larger, primarily because of long-range Coulombic interactions. The strong orientational dependence resulting from the point charges makes the methanol B_2 values especially negative at low temperatures, where highly attractive orientations are strongly preferred. These trends are observed at the higher orders as well.

Where the biconnected contribution B_n^{BC} is discernable from B_n in Fig. 2(b)–2(d), we plot it in red. With the scales selected, the non-biconnected contributions B_n^{NBC} are imperceptible for TraPPE-UA propane at all orders, and that of *n*-butane are visible only at fifth order. B_n^{NBC} is most visible near where B_n^{BC} goes through zero, in part because the scale magnifies differences near zero. To further examine the nature of B_n^{NBC}, we have plotted the ratio of it to the magnitude of B_n at third and fourth orders in Figs. 3 and 4, respectively. Overall, the relative significance of B_n^{NBC} to the alkane B_n increases with the chain length and the resulting increase in

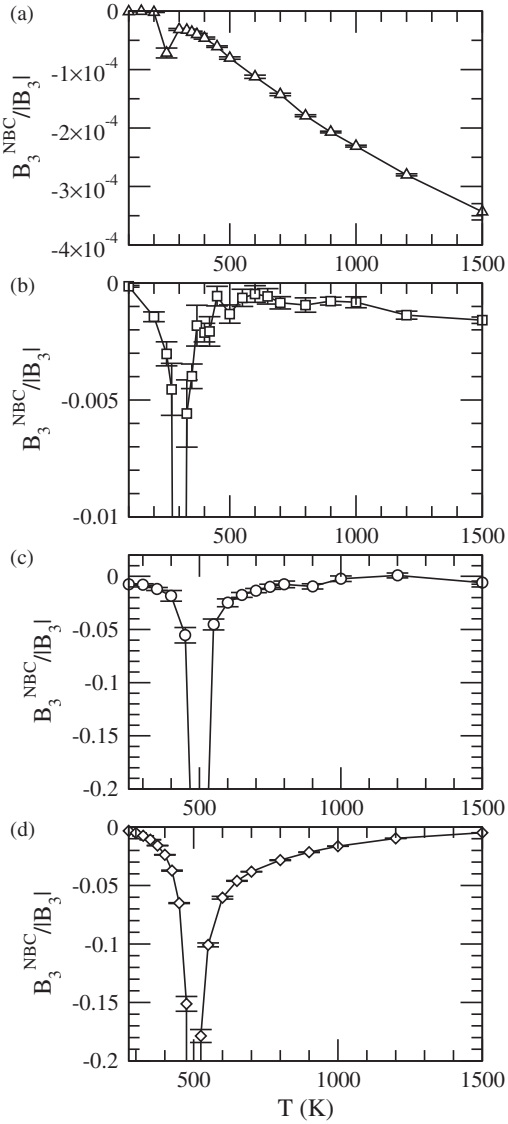

FIG. 3. Significance of the uniquely flexible contribution to B_3 for TraPPE-UA (a) propane, (b) *n*-butane, (c) *n*-dodecane, and (d) methanol. Error bars denote 68% confidence limits in the ratio.

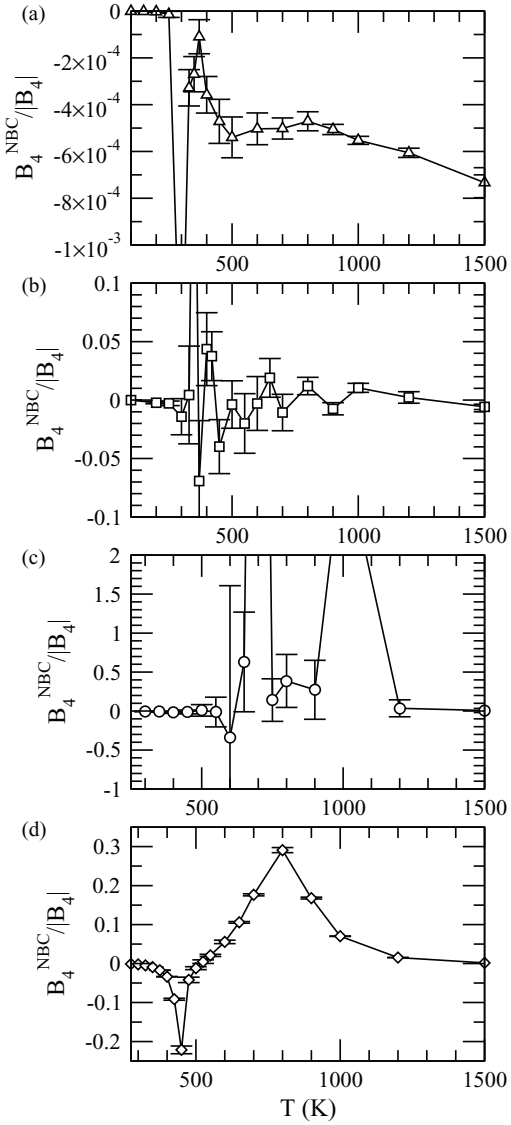

FIG. 4. Significance of the uniquely flexible contribution to B_4 for TraPPE-UA (a) propane, (b) *n*-butane, (c) *n*-dodecane, and (d) methanol. Error bars denote 68% confidence limits in the ratio.

possible intramolecular conformations. Though the propane and methanol models have the same number of sites per molecule, the significance of B_3^{NBC} and B_4^{NBC} is orders of magnitude larger for TraPPE-UA methanol. The strength of the site-site Coulombic interactions of the methanol model is likely responsible.

Caracciolo *et al.* proved that B_3^{NBC} is always negative,[3] which is what we observe in Fig. 3 at all data points but one: the dodecane data point at 1200 K, which we assume is positive only because of poor precision; its 68% confidence limit extends below the abscissa. For TraPPE-UA propane, the significance of B_3^{NBC} is small but measurable and increases with increasing temperature. Similar to the context of Boltzmann sampling, the molecules become more flexible with increasing temperature, in that a wider range of intramolecular conformations is important with regard to the Mayer functions. B_3^{NBC} for each model considered goes through zero somewhere in this temperature range, and the width of the resulting trough in $B_3^{NBC}/|B_3|$ obscures the effect of temperature for the models other than TraPPE-UA propane.

As a negative quantity, B_3^{NBC} reduces the pressure at a given density and temperature. The sign of B_3^{NBC} is perhaps a reflection of how molecular flexibility permits lower Boltzmann-averaged energies for given center-of-mass configurations. B_4^{NBC} is also negative for TraPPE-UA propane at all considered temperatures, as can be seen in Fig. 4, but becomes positive for TraPPE-UA methanol at a temperature between 500 and 525 K. For TraPPE-UA *n*-butane and *n*-dodecane, the uncertainties are too large on B_4^{NBC} to know the sign with confidence. As can been in Tables V–VIII of the supplementary material,[10] for all of the models considered, I_2F_3 is positive and the remainder of B_4^{NBC} is negative except at the highest temperatures. These contributions are difficult to compute precisely and largely cancel such that the sum is small and has poor precision.

B_n^{NBC} is more difficult to compute to high precision than B_n^{BC}, in part, because the non-biconnected diagrams have contributions from larger swathes of configuration space: the relative lack of connectivity increases the importance of larger separations. This configuration space grows with the number of molecules, and, though calculations for B_5^{NBC} of TraPPE-UA propane and *n*-butane were performed, these values are not yet known with confidence, as can be seen in Tables IX and X of the supplementary material.[10] We have found that computing B_n^{BC} together with the portion of B_n^{NBC} that omits disconnected diagrams with more than two parts (e.g., computing $-1/30I_5$ and $-F_5$ together) provides a modest improvement in the uncertainties of the total virial coefficient relative to computing these components separately. Including disconnected diagrams with more than two parts would require at least two alternate roots.

B. Vapor-branch spinodals and critical points

As shown in Fig. 5, the VEOS vapor-branch spinodals are almost indiscernible from those computed from the biconnected VEOS (VEOS BC), in which the uniquely flexible contributions are omitted. We terminate these spinodals, the loci of points at which the first derivative of the pressure with respect to density is zero, at the critical point, where the second derivative is also zero. The critical density ρ_c, critical temperature T_c, and critical pressure P_c for each considered model are presented in Table I for the VEOS and its biconnected approximation. With increasing order, the VEOS estimates of the critical properties approach the critical properties extrapolated from Gibbs-ensemble Monte Carlo simulation data.[6,7] These simulation values are in good agreement with those found experimentally for the modeled fluids.[11,12]

To estimate the uncertainty on a VEOS critical property x_c or a VEOS BC critical property x_c^{BC}, we employ 100 perturbations of the equation of state. Each perturbation is generated by sampling values of B_n (or B_n^{BC}) from Gaussian distributions centered at the average and having standard deviation equal to the standard error of this average. We then take the uncertainty of the critical property to be the standard error of its 100 perturbations. Rather than propagating the uncertainties of x_c and x_c^{BC} to estimate the uncertainty of the percent contribution of B_n^{NBC} to x_c, we apply this perturbation procedure directly to $(x_c - x_c^{BC})/x_c$, sampling B_n^{BC} and B_n^{NBC} independently. From the tabulated values, it can be seen that the differences between the complete and biconnected critical properties are statistically significant for TraPPE-UA propane and methanol at third and fourth order and *n*-dodecane at third order.

Where statistically significant, B_3^{NBC} increases VEOS3 estimates of ρ_c, T_c, and P_c relative to those of VEOS3 BC in accordance with its attractive effect: it decreases the region over which vapor is metastable or stable. For TraPPE-UA *n*-dodecane, B_3^{NBC} increases these VEOS3 properties by 1.29(17)%, 0.47(6)%, and 1.8(2)%, respectively, while for TraPPE-UA methanol, it increases these by 3.67(12)%, 1.04(3)%, and 4.67(15)%, respectively. The increases for

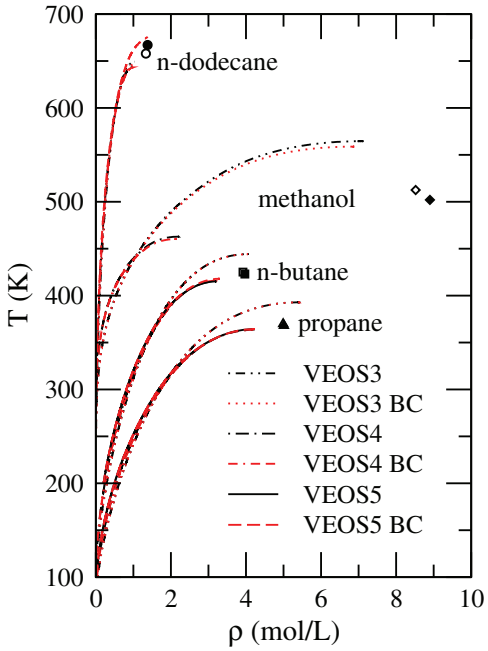

FIG. 5. Vapor-branch spinodals terminated at the critical point for VEOS3 (black dashed-dotted-dotted curve), VEOS3 BC (red dotted curve), VEOS4 (black dashed-dotted curve), VEOS4 BC (red dashed-dashed-dotted curve), VEOS5 (black solid curve), and VEOS5 BC (red dashed curve) of each considered TraPPE-UA model. Black symbols represent critical points extrapolated from Gibbs-ensemble Monte Carlo simulation data for the models considered (see Refs. 6 and 7), and white symbols represent critical points determined experimentally for the modeled fluids (see Refs. 11 and 12).

TraPPE-UA propane critical properties at both third and fourth order are less than 0.01%. For TraPPE-UA methanol, B_3^{NBC} and B_4^{NBC} together have percent contributions at fourth order that are about half those of B_3^{NBC} at third order. Even though B_4^{NBC}, like B_3^{NBC}, is negative within this temperature region, the VEOS4 critical point occurs at a lower temperature, where these contributions are smaller.

C. Corrections to previously published TraPPE-UA methanol virial coefficients

Previously published values[9] for TraPPE-UA methanol were computed using an oxygen-hydrogen bond length r_{OH} of 0.95 Å instead of the value 0.945 Å recommended for the model. This reduced the shielding of the hydrogen's positive charge by its bonded oxygen, allowing it to have more attractive interactions with other oxygen atoms than it would otherwise. The impact of this additional attraction is significant, indeed more so than the omission of the non-biconnected diagrams, increasing the magnitude of B_2, B_3, and B_4 and their components as shown in Table II. The significance is larger at lower temperatures, where attractive energy wells are most important relative to other configurations, and at higher order, where more molecules are considered. The extended bond more than doubles the magnitude of B_4 at 275 K.

A plot of the compressibility factor $Z = P/\rho kT$, computed using the recommended bond length along the saturated

TABLE I. Critical properties for TraPPE-UA models computed through the VEOS, computed through the bi-connected VEOS (VEOS BC), or extrapolated from the simulation data, and critical properties for the modeled fluids determined by experiment. Values in parentheses are 68% confidence limits on the rightmost digit(s).

Equation of state	Critical point ρ_c (mol/L)	T_c (K)	P_c (MPa)	Percent contribution of B_n^{NBC} ρ_c	T_c	P_c
			Propane			
VEOS3	5.4228(18)	392.85(9)	5.904(3)	0.00280(11)	0.00131(5)	0.00411(16)
VEOS3 BC	5.4227(17)	392.84(11)	5.904(3)			
VEOS4	4.179(7)	363.4(2)	4.405(8)	0.0040(13)	0.0017(4)	0.0054(16)
VEOS4 BC	4.179(7)	363.4(2)	4.405(8)			
VEOS5	4.22(5)	364.2(1.0)	4.44(5)	1.0(1.1)	0.2(3)	0.9(1.0)
VEOS5 BC	4.18(3)	363.4(6)	4.40(3)			
Simulation[a]	5.01(7)	368(2)	4.4(1)			
Experiment[b]	4.99(7)	369.83(10)	4.248(10)			
			n-Butane			
VEOS3	4.060(2)	444.22(19)	4.998(5)	0.04(3)	0.019(13)	0.06(4)
VEOS3 BC	4.0581(14)	444.13(12)	4.995(3)			
VEOS4	3.209(11)	415.2(4)	3.848(15)	−0.7(4)	−0.20(13)	−0.8(5)
VEOS4 BC	3.231(3)	415.98(14)	3.878(4)			
VEOS5	3.20(12)	415(3)	3.84(13)	−3(4)	−0.7(1.0)	−3(4)
VEOS5 BC	3.303(19)	418.0(5)	3.96(2)			
Simulation[a]	3.97(10)	423(4)	4.1(4)			
Experiment[b]	3.92(5)	425.12(10)	3.796(10)			
			n-Dodecane			
VEOS3	1.027(2)	649.3(5)	1.848(5)	1.29(17)	0.47(6)	1.8(2)
VEOS3 BC	1.0139(11)	646.3(3)	1.816(3)			
VEOS4	0.99(2)	643(3)	1.77(4)	−0.6(1.9)	0.1(4)	−0.2(1.9)
VEOS4 BC	0.991(4)	643.1(7)	1.775(8)			
VEOS5 BC	1.38(4)	675(3)	2.36(5)			
Simulation[a]	1.38(4)	667(5)	2.3(2)			
Experiment[b]	1.33(6)	658(1)	1.82(10)			
			Methanol			
VEOS3	7.13(3)	564.6(7)	11.15(7)	3.67(12)	1.04(3)	4.67(15)
VEOS3 BC	6.86(2)	558.7(5)	10.63(4)			
VEOS4	2.21(2)	463(1)	3.32(3)	2.2(2)	0.54(4)	2.7(2)
VEOS4 BC	2.160(17)	460.3(6)	3.23(3)			
Simulation[c]	8.90(12)	502(2)				
Experiment[d]	8.52(6)	512.5(2)	8.084(20)			

[a]Reference 7.
[b]Reference 11.
[c]Reference 6.
[d]Reference 12.

TABLE II. Ratios of TraPPE-UA methanol terms, $r_{OH} = 0.95$ Å to $r_{OH} = 0.945$ Å.

T (K)	B_2	B_3	B_3^{BC}	B_3^{NBC}	B_4	B_4^{BC}	$-1/2F_4^A - 3/2F_4^B - 3/2F_4^C$	$5/2I_2F_3$
275	1.16	1.50	1.50	1.35	2.18	2.18	1.73	1.56
300	1.13	1.43	1.43	1.30	1.95	1.95	1.61	1.47
325	1.11	1.38	1.38	1.24	1.85	1.85	1.51	1.38
350	1.10	1.34	1.34	1.22	1.73	1.74	1.43	1.33
375	1.08	1.32	1.32	1.18	1.70	1.70	1.36	1.28
400	1.07	1.31	1.31	1.16	1.70	1.71	1.32	1.24
425	1.06	1.31	1.32	1.14	2.00	2.07	1.28	1.22
450	1.06	1.35	1.36	1.12	0.14	0.37	1.25	1.18
475	1.05	1.50	1.57	1.10	1.06	1.08	1.22	1.16
500	1.05	− 9.01	− 0.57	1.09	1.16	1.17	1.22	1.15
550	1.04	0.95	0.96	1.08	1.19	1.20	1.17	1.13
600	1.04	1.01	1.02	1.08	1.19	1.21	1.16	1.10
650	1.04	1.03	1.03	1.06	1.19	1.21	1.17	1.11
700	1.04	1.03	1.03	1.07	1.14	1.20	1.27	1.09

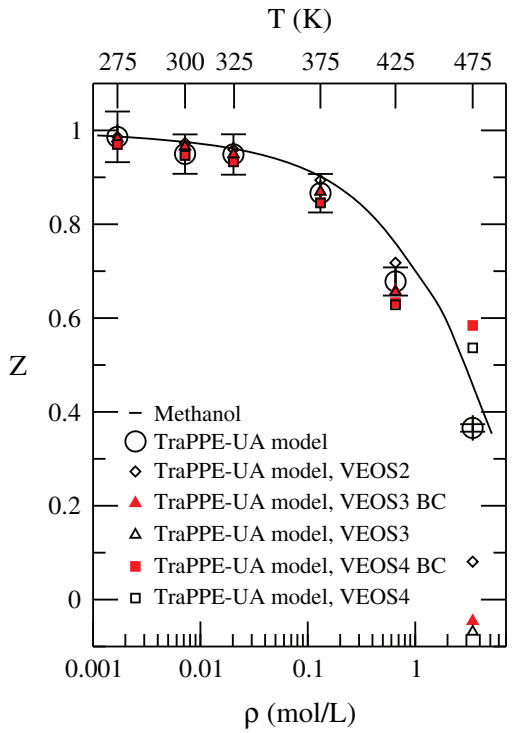

FIG. 6. The compressibility factor Z for TraPPE-UA methanol along the saturated vapor line assuming the saturated vapor densities and temperatures determined for the model by Gibbs-ensemble Monte Carlo simulation (see Ref. 6). These simulation data are represented with circles. VEOS2 values are represented with white diamonds, VEOS3 values with white triangles, VEOS3 BC values with red triangles, VEOS4 values with white squares, and VEOS4 BC values with red squares. The compressibility factor for methanol along its saturated vapor line (see Ref. 14) is represented with a black curve.

vapor line, is included in Fig. 6. The fourth-order contribution with the recommended bond length is less significant at low density, reflecting its appropriately smaller magnitude. The non-biconnected contributions, attenuated at low density like the biconnected contributions, become more apparent with increasing density and temperature, but VEOS3 and VEOS4 become inadequate with increasing density before the uniquely flexible contributions become apparent on this scale. At the highest temperature and density considered, the uniquely flexible contributions improve the VEOS3 and VEOS4 estimates of the model's compressibility factor.

IV. CONCLUDING REMARKS

The uniquely flexible contributions to the virial coefficients are in many instances negligible or small, but they can be significant and must be examined to ensure accuracy in calculated virial coefficients. Even when they are small, it can be difficult to compute them to the same precision as the biconnected contributions. We will continue to develop techniques that facilitate their computation in future work.

ACKNOWLEDGMENTS

This material is based upon work supported by the U.S. National Science Foundation under Grant Nos. CBET-0854340 and CHE-0626305. Calculations were performed using resources from the University at Buffalo Center for Computational Research.

[1]J. P. Hansen and I. R. McDonald, *Theory of Simple Liquids*, 2nd ed. (Academic Press, London/Orlando, 1986).
[2]S. Caracciolo, B. M. Mognetti, and A. Pelissetto, J. Chem. Phys. **125**, 094903 (2006).
[3]S. Caracciolo, B. M. Mognetti, and A. Pelissetto, Macromol. Theory Simul. **17**, 67 (2008).
[4]J. K. Singh and D. A. Kofke, Phys. Rev. Lett. **92**, 220601 (2004).
[5]K. M. Benjamin, A. J. Schultz, and D. A. Kofke, J. Phys. Chem. B **113**, 7810 (2009).
[6]B. Chen, J. J. Potoff, and J. I. Siepmann, J. Phys. Chem. B **105**, 3093 (2001).
[7]M. G. Martin and J. I. Siepmann, J. Phys. Chem. B **102**, 2569 (1998).
[8]A. J. Schultz and D. A. Kofke, J. Chem. Phys. **133**, 104101 (2010).
[9]K. R. S. Shaul, A. J. Schultz, and D. A. Kofke, Mol. Simul. **36**, 1282 (2010).
[10]See supplementary material at http://dx.doi.org/10.1063/1.3635773 for tabulated values of the virial coefficients and components thereof.
[11]D. Ambrose and C. Tsonopoulos, J. Chem. Eng. Data **40**, 531 (1995).
[12]M. Gude and A. S. Teja, J. Chem. Eng. Data **40**, 1025 (1995).
[13]A. J. Schultz and D. A. Kofke, Mol. Phys. **107**, 2309 (2009).
[14]E. W. Lemmon, M. O. McLinden, and D. G. Friend, "Thermophysical Properties of Fluid Systems" in *NIST Chemistry WebBook, NIST Standard Reference Database Number 69*, edited by P. J. Linstrom and W. G. Mallard (National Institute of Standards and Technology, Gaithersburg MD), http://webbook.nist.gov (retrieved June 1, 2011).